Proceedings of the 5th WSEAS Int. Conf. on SIGNAL, SPEECH and IMAGE PROCESSING, Corfu, Greece, August 17-19, 2005 (pp90-95)

Computationally Efficient Fingerprint Algorithm for Automatic Recognition

M.A. DABBAH, W.L. WOO, and S.S. DLAY
School of Electrical, Electronic and Computer Engineering
University of Newcastle
Newcastle upon Tyne, NE1 7RU
UNITED KINDOM

Abstract: - This paper presents a new computationally efficient fingerprint algorithm for automatic recognition (CEFAR). We use the Gabor filter to enhance the image before minutiae extraction within the sub-region in the fingerprint that was defined by the singularity point (SP). Accurate matching requires accurate extraction of minutiae and detection of SP. Conditional Number concept has been used after performing binarising and thinning operations in order to extract the minutiae from the enhanced fingerprint. For SP detection, core type was detected by using complex filtering applied to the orientation tensor field; this algorithm has been modified to reduce computational complexity. The matching methodology based on the star structure that is created using the minutiae and the SP. This structure is invariant with respect to global rotation and translation on the fingerprint due to the consistency of its formation. Comparing CEFAR to benchmark algorithms has shown that the CEFAR has maintained a high accuracy of EER less than 5%, together with dramatic reduction in the computation intensive requirements. There is a 60% reduction in SP detection and 41% of fingerprint image is only used for recognition, leading to a good efficiency.

Key-Words: - Biometric, Fingerprint, Singularity-Point, Tensor-Field, Gabor-Filter, Star-Notation

1 Introduction

Among all the biometric indicators, fingerprints have one of the highest levels of reliability, [1, 2], and have been extensively used by forensic experts in criminal investigations over a century.

Fingerprints are graphical ridge patterns present on human fingers that can be used for people identification due to their uniqueness and permanence [1, 2, 3]. A fingerprint is formed from an impression of the pattern of ridges on a finger [3]. A ridge is defined as a single curved segment, and a valley is the region between two adjacent ridges. Fingerprints can be described in two terms: global structure and local structure. Global structure refers to the flow pattern of the ridges that flow everywhere in the fingerprint and normally used for fingerprint classification. The local structure is described by the minutiae of the fingerprints, which are the local discontinuities in the ridge flow pattern. Minutiae can be described in terms of two fundamental types, ridge ending and bifurcation. Ridge endings are the points where the ridge lines terminate, and bifurcations are where the ridge lines split from a single path to two paths. They provide the sufficient amount of features to describe the uniqueness of the fingerprints. Hence they are intensively used for identification.

Local structure has been in different ways for identification. [4] uses a local texture analysis matching technique. Fingerprint feature vector is composed from the local information contained in each sector in a tessellated area of the image. The local information in each sector is decomposed into separate channels by using Gabor filter-bank. [4] concluded that although finger-codes are not as distinctive as minutiae, they carry complementary information that can be used together with minutiae to improve overall matching accuracy. [5] proposed interesting two-stage local minutiae matching algorithm where consolidation step is used to enforce the result of local matching. Local structure matching relies on the fact that local structure are characterised by attributes that are invariant with respect to the global rotation and translation, hence no global pre-alignment is required. It defines the local structure as a star graph notation for minutiae m_i in a given distance in the fingerprint. For each minutia m_j, in the defied distance from m_i, there is a vector e_{ij}. During matching, all stars of m_i are matched by a clockwise traversing the corresponding graphs in increasing order of radial angle φ_{ij} in the other fingerprint. We propose to use one star notation that corresponds to the SP in the pre-defined minutiae

area. This star notation is invariant with respect to global rotation and represents the template of the fingerprint. During matching, 1 to 1 star matching is performed instead of N to M star notations as in [5].

2 Minutiae Area Definition

The minutia area is defined by the core singularity type of the fingerprint. Hence, SP has to be detected, but before applying the detection algorithm, segmentation of the fingerprint foreground region is required in order to avoid detection of SP outside the ridge-valley pattern due to noise in the background.

2.1 Segmentation:

This uses the intensity variance of the fingerprints image. This is a block-wise operation that assigns each block WxW to foreground or background according to the variance of grey-levels in the image [6].

$$V(k) = \frac{1}{W^2} \sum_{i=0}^{W-1} \sum_{j=0}^{W-1} (I(i,j) - M(k))^2 \quad (1)$$

where $V(k)$ is the variance of intensity in the block k ,W is the block width, $M(k)$ is the mean value of intensity in the block k and $I(i,j)$ is the intensity value of the pixel (i,j) in the block k .

Fig1. Original and segmented images

This also reduces the area that is submitted to the SP detection algorithm.

2.1 SP Detection

SP's are defined as the orientation discontinuity of the flow field. There are two different SP's, delta and core. The core type is the inner point of the curving ridge flow while the delta is the meeting point of three different flow directions [7]. The detection algorithm uses complex filters that are applied to the orientation tensor field [8]. In the original algorithm, complex filtering is performed to the image in multi-resolutions scale by applying the complex filters to four levels of the multi-resolution Gaussian pyramid representation of the image, where the 3rd level is the lowest level of resolution and represents the global structure of the fingerprint image. However, we propose to apply the complex filters directly to the highest level only for locating the SP. This provides the similar results as using the multi-resolution filtering but with faster performance, since there is only one filtering operation that is performed on the one resolution-level. In addition, because we are interested in finding only one SP, which is the core type, we use one complex filter that is associated with the core type instead of using both types of complex filers as in the original approach.

$$C(x,y) = \exp\left\{-\frac{x^2+y^2}{2\sigma^2}\right\} \cdot (x+iy)^m \quad (2)$$

where the positive sign between the real and the imaginary parts in the second term is associated to the core type, m is the order of the filter and σ is the standard deviation of the Gaussian envelope. The filter is convolved with the orientation tensor field z at the highest resolution level, which is computed using the intensity gradients for each pixel in the x and y directions.

$$z(x,y) = (\partial G_x + i\partial G_y)^2 \quad (3)$$

Equation (3) is the tensor orientation field at pixel (x,y) . ∂G_x and ∂G_y are the gradients that are computed using the *sobel* operators. Before applying the filtering on the tensor field, we set its magnitude to unity so we use the angle of the field only. The core SP is detected at the maximum of the filtered orientation tensor field.

Once the SP is detected an area of NxM pixels around the core point is defined as the minutiae area.

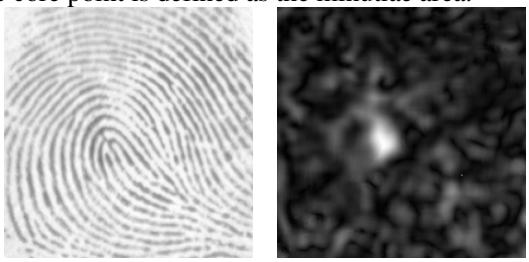

Fig2. Fingerprint and the complex filter response on the highest resolution level of the orientation tensor field

3 Fingerprint Image Enhancement

Normally, fingerprint images are presented in low quality images due to the degraded and corrupted ridge-valley pattern, which is affected by a noise that is generated from the variations in the skin and impression conditions.

3.1 Normalisation

It is required to maintain lower contrast images by standardising the intensity values of the pixels to a certain range of intensity variance around the mean. This obtains mean value of m_0 and variance of v_0 for the images submitted to the next enhancement process, and maintains balanced distribution between dark and light pixels, which reduces the effect of the distorted levels of variation in grey-level values along the ridges and valleys. This facilitates the subsequent image enhancement steps [9].

$$I'(i,j)=\begin{cases} m_0+\sqrt{(I(i,j)-M)^2\cdot v_0/v} & If \quad I(i,j)>m \\ m_0-\sqrt{(I(i,j)-M)^2\cdot v_0/v} & Otherwise \end{cases} \quad (4)$$

where $I(i,j)$ is the intensity value at pixel (i,j) and v is the variance of WxW block of the image and M is the mean value of that block.

3.2 Estimation of Local Ridge Orientation

In fingerprint, ridges and valleys alternate and flow in a locally constant orientations everywhere, called the local ridge orientation. The orientation field describes the coarse structure of a fingerprint and has been proven to be of a fundamental importance in fingerprint image processing [7]. Using the least mean square algorithm in [9], where the local orientation, θ_{ij}, of the block centred at pixel (i,j) is computed by:

$$\xi=\frac{2\sum_{u=i-\frac{W}{2}}^{i+\frac{W}{2}}\sum_{v=j-\frac{W}{2}}^{j+\frac{W}{2}}\partial G_x(u,v)\cdot\partial G_y(u,v)}{\sum_{u=i-\frac{W}{2}}^{i+\frac{W}{2}}\sum_{v=j-\frac{W}{2}}^{j+\frac{W}{2}}\partial G_x(u,v)^2-\sum_{u=i-\frac{W}{2}}^{i+\frac{W}{2}}\sum_{v=j-\frac{W}{2}}^{j+\frac{W}{2}}\partial G_y(u,v)^2} \quad (5)$$

$$\theta_{ij}=90°+\frac{1}{2}\arctan(\xi) \quad (6)$$

Furthermore, the orientation field is smoothed by convolving the continues x and y vector field components in equations (7) and (8), respectively, with a law-pass Gaussian filter. Then the smoothed orientation field is calculated by equation (9), where $\Phi'_x(i,j)$ and $\Phi'_y(i,j)$ are the smoothed continues x and y vector field components.

$$\Phi_x(i,j)=\cos(2\theta_{ij}) \quad (7)$$

$$\Phi_y(i,j)=\sin(2\theta_{ij}) \quad (8)$$

$$\theta'_{ij}=\frac{1}{2}\arctan\left(\frac{\Phi'_y(i,j)}{\Phi'_x(i,j)}\right) \quad (9)$$

3.3 Estimation of Local Ridge Frequency

For different regions in the fingerprint image the pattern of ridges follows with different spatial frequencies. The frequency is estimated by projecting the intensity values in the orthogonal direction of the flow pattern of ridges [9]. The projection gives a sinusoidal waveform, this waveform is low pass filtered to maintain well defined peaks that indicate the ridge lines in order to estimate the frequency more accurately. Then, the local frequency for the block WxW centred at pixel (i,j) is defined as the average number of pixels between two peaks in the smoothed sinusoidal wave formed by the projection.

3.4 Spatial Domain Filtering (Gabor Filtering)

This is based on the convolution of the image with the even-symmetric Gabor filters that are tuned to the local ridge orientation and ridge frequency [9, 10]. The employed Gabor filters are two-dimensional band-pass filters that are consisted of a sinusoidal plane wave with certain orientation and frequency, modulated by a Gaussian envelope [9].

$$G(x,y;\theta,f)=\exp\left\{-\frac{1}{2}\left[\frac{x_\theta^2}{\sigma_x^2}+\frac{y_\theta^2}{\sigma_y^2}\right]\right\}\cos(2\pi f x_\theta) \quad (10)$$

$$x_\theta=x\cos\theta+y\sin\theta \quad (11)$$

$$y_\theta=-x\sin\theta+y\cos\theta \quad (12)$$

Fig3. Original and filtered images using the method in [9]

4 Feature Extraction

After enhancing the fingerprint image, minutia points are represented in clearer form and can be extracted in order to form the fingerprint code (fingerprint features). Note that the quality of the extracted fingerprint features is dependant on the quality of the enhanced images. To be able to extract the minutiae from the enhanced image, it has to be converted into a thinned form from the binary image.

4.1 Binarisation

In the binary representation there are only two different values, 0's and 1's where 0's present ridges and 1's present valleys. Binarisation works by setting the values of the pixels in the image to zero or one according to a threshold value. The ridges and valleys have distinguished from each other very clearly by the Gabor filter, hence a local threshold binarisation method that is followed by open, eroding, dilating and closing morphological operators guarantees a satisfactory result. Morphological operators are used to eliminate islands (separate pixels) and noises between ridges, which reduces number of spikes in the thinned image.

4.2 Thinning (Skeletonisation)

Once the binary image is available, the skeleton is obtained by performing an intermediate thinning step. The algorithm in [11] is used. It successively erodes away the foreground pixels from the binary image using two sub-iterations. These sub-iterations inspect the neighbourhood of each pixel in the binary image and delete the pixel if it can be deleted. This deletion decision is based on specific criteria defined by the algorithm. The sub-iterations continue until no more pixels can be deleted and all the ridges are one pixel wide (skeleton).

4.3 Condition Number

The minutiae are extracted by scanning the local neighbourhood of each pixel in the skeleton image using a $3x3$ window. The condition number value is then computed as in [6], and according to the computed value, the ridge pixel can be classified as a ridge-ending, bifurcation or non-minutia point. Any pixel in the skeleton image that has a value equal to one is classified as ridge-ending point, and equal to three is classified as bifurcation. Otherwise it is considered as non-minutiae point. The condition number for a ridge pixel P is given by:

$$CN(P) = \frac{1}{2}\sum_{i=1..8}\left|val(P_{i \bmod 8}) - val(P_{i-1})\right| \quad (13)$$

where Pi is the pixel value in the neighbourhood of P. The eight neighbouring pixels of the pixel P are scanned in a clockwise or anti-clockwise direction.

4.4 The Extracted Minutiae Information

1) The Euclidean Distance between the extracted minutia and the reference points.

$$D_e = \sqrt{(x_r - x_m)^2 + (y_r - y_m)^2} \quad (14)$$

where (x_r, y_r) is the SP and (x_m, y_m) is the minutia point.

2) The orientation of the associated ridge segment with respect to the reference point which is the difference between the orientation of the extracted minutia and the orientation of the reference point.

$$\theta_e = \min\left(\left|\theta_r - \theta_m\right|, 360 - \left|\theta_r - \theta_m\right|\right) \quad (15)$$

where θ_r and θ_m are the orientation of the SP and the extracted minutia point respectively.

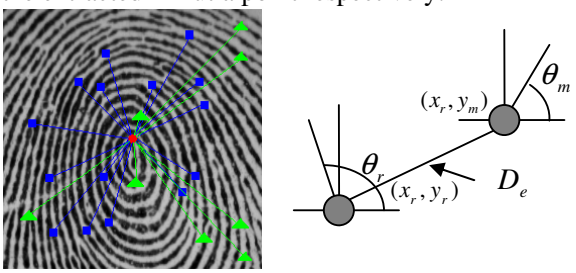

Fig4. The star notation that presents the template of the fingerprint and its formation

The equation takes the minimum because of the circularity of angles.

3) The type of minutiae, which simply indicates whether the extracted minutia point is ridge ending or bifurcation. These three elements form the minutiae vector, which the basic component in and forms the star matching structure.

5 Matching

For each minutia vector in the template there are three elements: distance, orientation with respect to SP and type (bifurcation and ridge ending). For illustration, template is donated by T and input fingerprint is donated by I. The template has M minutia points, where the input fingerprint has N points:

$$T = \{m_1, m_2, ..., m_M\}, \quad (16)$$

$$m_i = \{sd_i, od_i, type_i\}, \quad i = 1..M \quad (17)$$

$$I = \{m'_1, m'_2, ..., m'_N\}, \quad (18)$$

$$m'_j = \{sd_j, od_j, type_j\}, \quad j = 1..N \quad (19)$$

where m_i and m_j are minutia points in T and I respectively. For two minutiae to be matched, both minutia vectors have to be within the same the tolerance box (hyper-spheres) defined by r_0 and θ_0, which means that:

$$De_i - De_j \le r_0 \quad (20)$$

and $$\theta e_i - \theta e_j \le \theta_0 \quad (21)$$

where De_i, De_j and θe_i, θe_j are the Euclidean distances and the orientation differences of the

minutiae m_i and m_j from the SP respectively. It should be noted that pre-defined r_0 and θ_0 are added to tolerate elastic distortion errors during fingerprint acquisition process. In addition, minutiae have to be in the same type, ridge ending or bifurcation, in order to match.

$$type_i = type_j \quad (22)$$

This matching methodology can be modelled as star matching algorithm, where for each fingerprint there is one individual star graph that is formed by the minutiae vectors and invariant with respect to the global rotation and translation on the fingerprint due to the reference to the SP.

6 Results

The benchmark database used in these experiments was obtained from DB2 set A of FVC2000 [12]. Each fingerprint image is in TIFF format, 8-bits grey level and scanned at 500dpi resolution and of size 300x300 pixels using a low-cost optical sensor.

A total of 800 fingerprint (100 persons, eight fingerprints per person, many of which are of a poor quality.

To evaluate the FRR (False Rejection Rate), the first image of each fingerprint is matched with the first image of the other fingerprints and for evaluating FAR (False Acceptance Rate), each image is matched with the other seven images of the same fingerprint The EER (Equal Error Rate) is when FRR and FAR are equal. The performance results are shown in Figure 5 and 6.

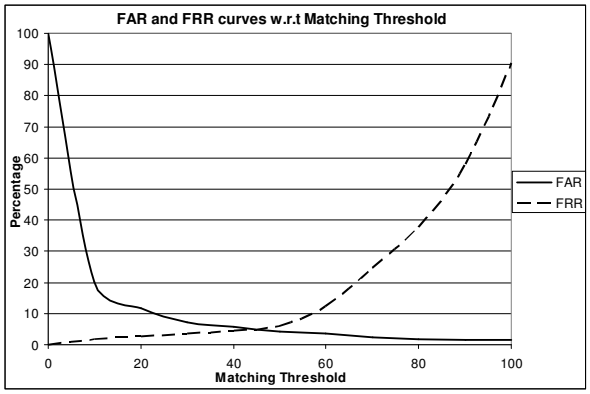

Fig5. FAR and FRR curves with respect to the matching threshold as percentage from the matched minutiae

From figure 5 and 6, the EER is at 4.9% when the matching threshold is 45% of the minutiae points. The matching threshold indicates the number of minutiae matched (in percentage) from one fingerprint with another one. The number of steps in the SP detection algorithm is significantly reduced, 60% of the original, without leading to significant reduction of the accuracy. In addition, the minutiae area that has been defined by the SP is only 41% of the original size of the image. These reduce the processing requirement for the system to enrol a fingerprint.

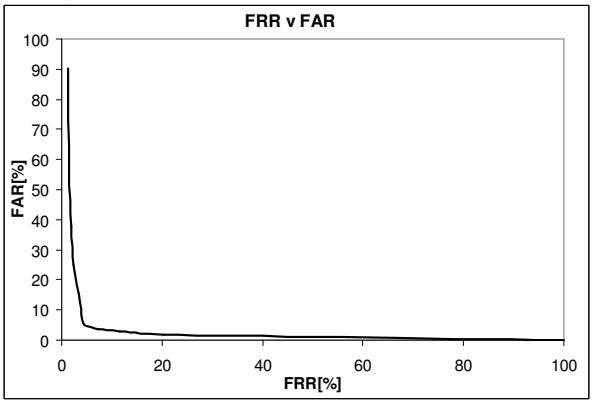

Fig6. FRR plotted against the FAR (the ROC curve).

Furthermore, the matching mechanism of comparing one star structure per fingerprint has reduced the complexity of matching, since there is only one star structure per fingerprint. Therefore CEFAR meets high security requirements, as the EER is less than 5%, with reliable online recognition system.

Algorithm	***CEFAR***	*Cetp*	*Utwe*	*Diti*	*Ncmi*
EER[%]	**4.9**	5.06	7.98	23.64	49.11
CEFAR accuracy improvement over others [%]	**----**	3.27	62.86	382.45	902.24

Table1. Comparison with other algorithms from [12]

Table 1 performs a comparison with other benchmark algorithms [12], the comparison shows that CEFAR performs the other algorithms, which is also less computational intensive. The accuracy improvement over the *Ncmi* is 902.24%, which is dramatically high, and the average improvement of accuracy over all the algorithms is 337.7%.

7 Conclusion

In this work we present a high efficiency combined accuracy fingerprint recognition algorithm. The algorithm defines a minutiae area using the SP of the fingerprint, where the complexity of detecting the SP is reduced by 60%. The algorithm performs fingerprint image enhancement on this defined minutiae area, which is 41% of the original fingerprint image, in order to obtain accurate minutiae extraction. Also the complexity of matching is significantly reduced by using the SP. These

computation reductions have developed a reliable algorithm that also maintains high accuracy performance as shown by EER less than 5% together with an average accuracy improvement over benchmark algorithms of 337.7%.

8 Acknowledgment

The authors would like to acknowledge the financial support of the Office of the Deputy Prime Minister (ODPM) under the project "Developing Authentications Tokens for Electronic Access" (DATES).

References:

[1] L. O'Gorman, "Comparing Passwords, Tokens, and Biometrics for User Authentication," *Proceedings of the IEEE,* vol. 91, no. 12, pp.2021-2040, December 2003

[2] J. Zhou, J. Gu,"A Model-Based Method for the Computation of Fingerprints' Orientation Field," *IEEE Transaction on Image Processing*, vol. 13, no. 6, pp. 821-835, June 2004

[3] M. Tico, P. Kuosmanen, "Fingerprint Matching Using an Orientation-Based Minutia Descriptor," *IEEE Transaction on Pattern Analysis and Machine Intelligence,* vol. 25, no. 8, pp. 1009-1014, Aug 2003

[4] Jain A.K., Prabhakar S., Hong L., and Pankanti S., "Filter-bank-Based Fingerprint Matching," *IEEE Transaction on Image Processing*, vol. 9, pp. 846-859, 2000

[5] Ratha N.K., Pandit V.D., Bolle R.M., and Vaish V., "Robust Fingerprint Authentication Using Local Structural Similarity," in *Proc. Workshop on Application of Computer Vision*, pp. 29-34, 2000

[6] Mehtre B. M., "Fingerprint image analysis for automatic identification," *Machine Vision and Applications*, vol. 6, no. 2-3, pp.124–139, 1993

[7] Dass S.C., "A Markov Random Field Models for Directional Field and Singularity Extraction in Fingerprint Image," *IEEE Transaction on Image Processing,* vol. 13, no. 11, pp. 1358-1367, Nov. 2004

[8] Kenneth Nilsson and Josef Bigun, "Localization of corresponding points in fingerprints by complex filtering," *Pattern Recognition Letters*, vol. 24, pp. 2135-2144, 2003

[9] Hong L., Wan Y., and Jain A.K., "Fingerprint Image Enhancement Algorithms and Performance Evaluation," *IEEE Transaction on Pattern Analysis and Machine Intelligence,* vol. 20, no.8, pp. 777-789, 1998

[10] J. Yang, L. Liu, T. Jiang, Y. Fan, "A modified Gabor filter design method for fingerprint image enhancement," *Pattern Recognition Letters,* vol. 24, no 12, pp. 1805–1817, Aug 2003

[11] Louisa Lam, Seong-Whan Lee, and Ching Y. Wuen, "Thinning Methodologies-A Comprehensive Survey," *IEEE Transaction on Pattern Analysis and Machine Intelligence*, vol. 14, no. 9, pp. 869-885, 1992

[12] Maio, D., Maltoni, D., Cappelli, R., Wayman, J.L., Jain, A.K., "FVC2000: Fingerprint Verification Competition," *IEEE Transaction on Pattern Analysis and Machine Intelligence*, 24 (3), 402–412, 2002